

Deep-sea reverse osmosis desalination for energy efficient low salinity enhanced oil recovery

Original

Deep-sea reverse osmosis desalination for energy efficient low salinity enhanced oil recovery / Fasano, M.; Morciano, M.; Bergamasco, L.; Chiavazzo, E.; Zampato, M.; Carminati, S.; Asinari, P.. - In: APPLIED ENERGY. - ISSN 0306-2619. - ELETTRONICO. - 304:(2021), p. 117661. [10.1016/j.apenergy.2021.117661]

Availability:

This version is available at: 11583/2925594 since: 2021-09-20T14:14:16Z

Publisher:

Elsevier Ltd

Published

DOI:10.1016/j.apenergy.2021.117661

Terms of use:

This article is made available under terms and conditions as specified in the corresponding bibliographic description in the repository

Publisher copyright

Elsevier postprint/Author's Accepted Manuscript

© 2021. This manuscript version is made available under the CC-BY-NC-ND 4.0 license
<http://creativecommons.org/licenses/by-nc-nd/4.0/>. The final authenticated version is available online at:
<http://dx.doi.org/10.1016/j.apenergy.2021.117661>

(Article begins on next page)

Deep-sea reverse osmosis desalination for energy efficient low salinity enhanced oil recovery

Matteo Fasano^{a,b}, Matteo Morciano^{a,b}, Luca Bergamasco^a, Eliodoro Chiavazzo^a, Massimo Zampato^c, Stefano Carminati^d, Pietro Asinari^{a,e}

^aDepartment of Energy, Politecnico di Torino, C.so Duca degli Abruzzi 24, Torino 10129, Italy

^bClean Water Center, Politecnico di Torino, C.so Duca degli Abruzzi 24, Torino 10129, Italy

^cENI S.p.a., Via Pacinotti, 4, 30175 Venezia, Italy

^dENI S.p.a., Via F. Maritano 26, 20097 San Donato Milanese (Mi), Italy

^eIstituto Nazionale di Ricerca Metrologica, Strada delle Cacce 91, Torino 10135, Italy

Abstract

The decrease in the oil discoveries fuels the development of innovative and more efficient extraction processes. It has been demonstrated that Enhanced Oil Recovery (EOR, or tertiary recovery technique) offers prospects for producing 30 to 60% of the oil originally trapped in the reservoir. Interestingly, oil extraction is significantly enhanced by the injection of low salinity water into oilfields, which is known as one of the EOR techniques. Surface Reverse Osmosis (SRO) plants have been adopted to provide the large and continuous amount of low salinity water for this EOR technique, especially in offshore sites. In this article, we outline an original solution for producing low salinity water for offshore EOR processes, and we demonstrate its energy convenience. In fact, the installation of reverse osmosis plants under the sea level (Deep-Sea Reverse Osmosis, DSRO) is found to have significant potential energy savings (up to 50%) with respect to traditional SRO ones. This convenience mainly arises from the non-ideality of reverse osmosis membranes and hydraulic machines, and it is especially evident – from both energy and technological point of view – when the permeate is kept pressurized at the outlet of the reverse osmosis elements. In perspective, DSRO may be a good alternative to improve the sustainability of low salinity EOR.

Keywords: Energy Efficiency, Water, Desalination, Reverse Osmosis, Enhanced Oil Recovery

1. Introduction

During the last decades, a decrease in the oil discoveries led to propose novel and more effective extraction methods to meet the growing energy demand. Therefore, Enhanced Oil Recovery (EOR, or tertiary recovery) technologies are nowadays gaining increasing attention to improve the efficiency of crude oil extraction from oilfields [1–4]. According to the US Department of Energy, EOR can extract about 30 to 60% of the oil trapped in the geological formation, whereas primary and secondary recovery not more than 20 to 40%.

EOR can be obtained by means of different techniques, depending on the oil type and geology of the oil reservoir [5]. Miscible processes, chemical floods and steam-based methods are exploited to reduce the interfacial tension between oil and injected water, therefore the capillary forces in the porous media. This improves the residual trapped oil displacement from the pores space, leading to an increased recovery perfor-

mance [6, 7]. Several additives (*i.e.* surfactants) can be added to tailor the composition of the injected fluid, and thus the ionic strength between the latter and oil [8, 9]. Hirasaki and co-workers, Sun and co-workers and Ge and co-workers, in their review [10] and research works [11, 12], respectively, have discussed the process of injecting alkali to generate soap in situ by reaction in the crude oil or synthetic surfactant to reduce the interfacial tension enabling an easier oil displacement.

Recently, the use of functionalized nanomaterials (e.g., nanoparticles, silica and graphene-based nanosheets) has received attention from the scientific community because of their effect on the remobilization of trapped oil [13, 14]. Pak and co-workers provided insights on the dynamics of nanoparticles used to remove organic fluids (e.g., oil) from porous media [15]. Several nanoparticles have been investigated (including Al₂O₃, TiO₂, ZnO, Fe₂O₃, and SiO₂) [16] and, among these, silica ones have shown better perfor-

mance. In detail, the large effect of mineral surfaces on wettability is reported in several studies [17, 18]. In fact, once adsorbed on the rock, the nanoparticles affect the capillary forces that trap oil in the pores as experimentally demonstrated by Zhang and co-workers [19], Suleimanov and co-workers [20] and Hendraningrat and co-workers [21], thus enabling flow even in small pores otherwise inaccessible [22–27]. Zhang and co-workers, for example, demonstrated that carbon nanosheets are able to recover about 20% more oil than the base brine [6].

Another exploited technique, which had arisen to the attention in 1967 [28], involves the injection of low salinity water into the oilfield. This process has been proved to improve crude oil extraction up to 40% [29]. In fact, Aziz and co-workers numerically assessed a relevant wettability alteration at the oil-water interface due to the introduction of low salinity water in the oil reservoir [28]. While the injection of freshwater may be convenient in case of ground or onshore installations – at least where water scarcity is not an issue [30], offshore installations may be supplied of low salinity water by either ship transport from the mainland or by sustainable desalination plants [31–35] installed on-board the oil platform. Surface Reverse Osmosis (SRO) desalination plants [36–38] could be typically adopted for these offshore EOR applications, because of their superior energy performance [39], broader commercial availability and easier industrial scalability [40] with respect to other desalination technologies. However, the energy and economic impact of the desalination process on the overall convenience of low salinity EOR may represent a substantial barrier for a widespread diffusion of this EOR solution. The potential of this method was first experimentally demonstrated by Tang and Morrow [41]. In their research work, an approximately 15% additional oil was produced reducing the salinity of the injecting water [41]. Later, other studies confirmed by means of experiments the enhanced oil recovery due to the variation of the capillary pressure [42] and permeability [43, 44] by low salinity water injection [45–48]. However, it is worth to point out that low salinity EOR is an energy intensive process, since it involves the installation of high-pressure pump to allow the water flow into the geological formation with the goal of displacing hydrocarbons. Then, it is extremely important to operate in a smart way to lower the energy consumption. To this purpose, in 2020, Janson and co-workers [49] conducted a techno-economic evaluation of a promising configuration where a pressure retarded osmosis device was coupled with EOR. The direct injection of produced water and of permeate from a pressure retarded osmo-

sis device have been compared, and a 38% decrease in the specific pumping energy (kWh m^{-3}) of the latter observed.

In this article, the aim is to explore an innovative way to produce low salinity water for EOR with energy and operational efficiencies superior to current solutions. In detail, here we perform a feasibility analysis of reverse osmosis systems located at the seabed (Deep-Sea Reverse Osmosis, DSRO), in correspondence of offshore oilfields. The desalinated water produced by this innovative DSRO process is then injected into the oil reservoir, to enhance oil extraction. The idea is to exploit the hydrostatic pressure of deep-sea seawater to achieve higher energy and operational efficiencies respect to existing SRO plants.

Despite some works in the literature have already proposed reverse osmosis desalination for human habitats at the seabed [50, 51] and performed energy calculations to study desalination under the sea [52, 53], to the best of the authors' knowledge, this work represents a first attempt to target energy efficient reverse osmosis to produce subsea low salinity water for EOR. Therefore, the novel aspects proposed in this article are: i) the evaluation of the thermodynamic convenience of a deep-sea reverse osmosis applied to enhanced oil recovery; ii) the assessment of its technical feasibility based on realistic case studies of interest to oil and gas companies; iii) the exploration of its optimal configurations in a systematic way via a detailed parametric analysis of the most relevant design features.

First, the energy convenience of DSRO with respect to SRO is discussed for ideal systems; second, a case study of DSRO for EOR is sized and analyzed under realistic conditions. The case study considers a set of design constraints of engineering interest for representative EOR applications, namely to be able to inject $1000 \text{ m}^3 \text{ day}^{-1}$ of low salinity water ($\text{TDS} < 5 \text{ mg L}^{-1}$, being TDS the total dissolved solids) in an oilfield located 1000 m under the sea level. Finally, the effect of recovery ratio, seabed depth, low salinity volumetric flow, efficiency of hydraulic machines, pressure losses and pressurized permeate at the outlet of RO units is explored by sensitivity analyses, to evaluate the optimum operating conditions for DSRO plants.

2. Methods

In this Section, SRO and DSRO plants designed for offshore EOR applications are described and schematically represented by block diagrams. The governing equations of these plants are then presented, with the

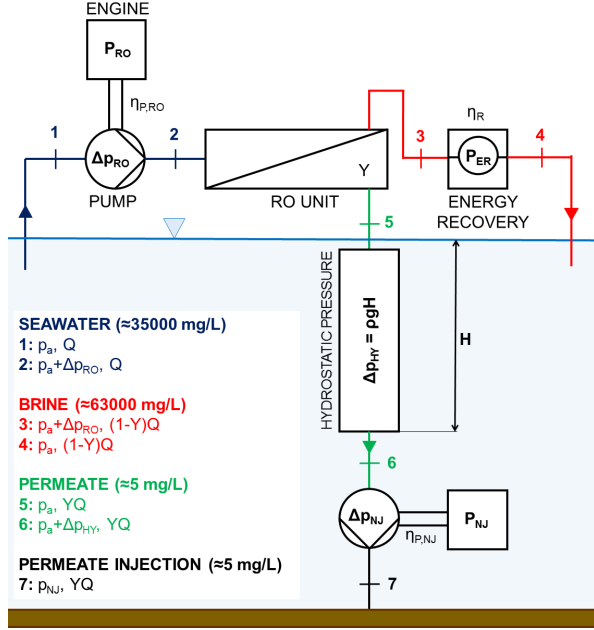


Figure 1: Schematic of a reverse osmosis plant for EOR located above the sea level (Surface Reverse Osmosis, SRO). Hydraulic connections between elements are differently colored according to the flowing fluid: seawater (blue, $\text{TDS} \approx 35000 \text{ mg L}^{-1}$); brine (red, $\text{TDS} \approx 63000 \text{ mg L}^{-1}$); permeate water (green or black, $\text{TDS} \approx 5 \text{ mg L}^{-1}$). The inlet/outlet of each element in the schematic is numbered, with the corresponding pressure and volumetric flow of the fluid specified in the white text box at the bottom left. Note that the indicated pressures do not consider pressure losses (ideal case).

aim to achieve an overall comparison between SRO and DSRO energy performances.

2.1. Ideal surface reverse osmosis

First, let us consider a traditional reverse osmosis plant located above the sea level (SRO). As a first approximation, both distributed and localized pressure losses in the system are neglected (ideal conditions).

As sketched in Fig. 1, a SRO plant for EOR applications can be subdivided into four main components: (i) a pump to pressurize seawater at the inlet of RO unit; (ii) a RO unit; (iii) an energy recovery system; (iv) a pump to inject permeate (distilled) water into the oilfield [54]. The first pump (with $\eta_{P,RO}$ hydraulic efficiency) allows to increase the pressure of a volumetric flow (Q) of seawater ($\text{TDS} \approx 35000 \text{ mg L}^{-1}$) from ambient conditions (p_a) to the pressure needed for RO process ($p_{RO} = p_a + \Delta p_{RO}$, being Δp_{RO} the pressure difference at the RO membrane). The RO unit can be made of several desalination stages, but the overall result is the production of brine ($\text{TDS} \approx 63000 \text{ mg L}^{-1}$) and perme-

ate ($\text{TDS} \approx 5 \text{ mg L}^{-1}$) water. The characteristic recovery ratio (Y) of the RO unit determines the volumetric flow of brine ($((1-Y)Q$) and permeate water (YQ). For better energy performance, the residual pressure of brine ($p_a + \Delta p_{RO}$ in the ideal case) is generally used to power energy recovery devices (e.g., Francis turbines or pressure exchangers, with η_R efficiency); brine is finally released into the sea at ambient conditions. Permeate water, instead, is collected in a submersed pipe connecting the SRO plant with the injection pump (with $\eta_{P,NJ}$ hydraulic efficiency), which is typically located at the seabed. This pump increases the permeate pressure up to the value requested for oilfield injection (p_{NJ}). However, the hydrostatic head in the submersed pipe ($\Delta p_{HY} = \rho g H$, where ρ is the water density, g the acceleration of gravity and H the sea depth) contributes to pressurize permeate water at the inlet of injection pump ($p_a + \Delta p_{HY}$); therefore, the actual pressure jump delivered by the injection pump can be roughly estimated as $\Delta p_{NJ} = p_{NJ} - (p_a + \Delta p_{HY})$.

The total power needed by the EOR process can be then estimated from an overall balance of the system, namely

$$P_{I,GR} = (P_{RO} - P_{ER}) + P_{NJ} = P_{GR} + P_{NJ} \quad (1)$$

where $P_{GR} = P_{RO} - P_{ER}$ is the net power needed by the RO process above the sea level (SRO). In Eq. 1, the power required by the reverse osmosis pump can be estimated as

$$P_{RO} = \frac{Q \Delta p_{RO}}{\eta_{P,RO}}, \quad (2)$$

the power generated by the energy recovery device as

$$P_{ER} = \eta_R (1 - Y) Q \Delta p_{RO}, \quad (3)$$

while the power required by injection pump as

$$P_{NJ} = \frac{Y Q \Delta p_{NJ}}{\eta_{P,NJ}}. \quad (4)$$

Note that a configuration with the injection pump positioned above the sea level does not alter the power balance in Eq. 1.

2.2. Ideal deep-sea reverse osmosis

The novel deep-sea reverse osmosis (DSRO) concept plant with no pressurized permeate is then considered. Again, both distributed and localized pressure losses in the system are initially neglected.

Figure 2 depicts a general schematic of the DSRO plant for offshore, low salinity EOR, where four main components are represented: (i) a pressure regulator at

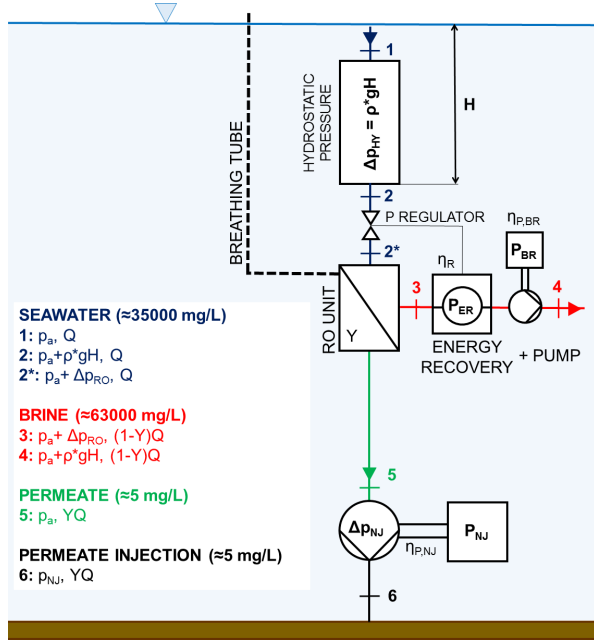


Figure 2: Schematic of a reverse osmosis plant for EOR located at the seabed (Deep-Sea Reverse Osmosis, DSRO). Hydraulic connections between elements are differently colored according to the flowing fluid: seawater (blue, TDS ≈ 35000 mg L⁻¹); brine (red, TDS ≈ 63000 mg L⁻¹); permeate water (green or black, TDS ≈ 5 mg L⁻¹). The black dashed line represents the breathing tube, which connects RO units with the ambient pressure. The inlet/outlet of each element in the schematic is numbered, with the corresponding pressure and volumetric flow of the fluid specified in the white text box at the bottom left. Note that the indicated pressures do not consider pressure losses (ideal case).

the inlet of RO unit; (ii) a RO unit; (iii) a brine re-pressurization system; (iv) a pump to inject permeate (distilled) water into the oilfield. The pressure regulator reduces seawater pressure at the seabed from hydrostatic values ($p_a + \Delta p_{HY}$, with $\Delta p_{HY} = \rho^*gH$ and ρ^* the density of salt water) to the maximum pressure supportable by RO units with no pressurized permeate ($p_{RO} = p_a + \Delta p_{RO}$). The inlet volumetric flow of seawater (Q) is processed by the RO unit and, thus, brine $((1-Y)Q)$ and permeate water (YQ) flows are produced. Under deep-sea conditions, brine needs then to be re-pressurized before being discharged into the sea. For better energy performance, the re-pressurization of brine from p_{RO} to $(p_a + \Delta p_{HY})$ can be carried out by the concurrent action of an energy recovery device (actuated by the pressure regulator, with η_R efficiency) and an auxiliary pump (with $\eta_{P,BR}$ efficiency). Thanks to a breathing tube connecting the RO units with the atmosphere, permeate water flows out from the RO unit at ambient pressure (p_a), and it is then injected into the

oilfield by an injection pump (with $\eta_{P,NJ}$ hydraulic efficiency). This pump increases the permeate pressure up to the value requested for oilfield injection (p_{NJ}), with a resulting pressure jump equal to $\Delta p_{NJ} = p_{NJ} - p_a$ (*i.e.* negligible additional hydrostatic head at the permeate side).

The total power needed by the EOR process can be then estimated from an overall balance of the system, namely

$$P_{L,DS} = (P_{BR} - P_{ER}) + P_{NJ} = P_{DS} + P_{NJ}, \quad (5)$$

where $P_{DS} = P_{BR} - P_{ER}$ is the net power needed to re-pressurize the discharged brine, thus the net power demand of the DSRO process under the hypothesis of ideal conditions. In Eq. 5, the power required by the auxiliary pump for brine re-pressurization is

$$P_{BR} = \frac{(1-Y)Q(\Delta p_{HY} - \Delta p_{RO})}{\eta_{P,BR}}, \quad (6)$$

the power generated by the energy recovery device is

$$P_{ER} = \eta_R Q (\Delta p_{HY} - \Delta p_{RO}), \quad (7)$$

while the power required by injection pump (P_{NJ}) is the same as Eq. 4.

2.3. Pressure losses and pressurized permeate

The hypotheses assumed for both SRO and DSRO plants in the previous Sections do not consider the following effects:

- performance curves of the pumps (η_P vs. Q);
- distributed and localized pressure losses;
- pressurized permeate (*i.e.* $p > p_a$).

On the one side, the effect of variable pump efficiency with the volumetric flow is strongly dependent on the technical solution adopted and, in any case, is equally affecting both SRO and DSRO plants. On the other side, pressure losses and permeate pressurization may lead to substantial differences between the surface and deep-sea solutions and thus are worth to be investigated.

While the DSRO plant should be typically close to the injection pump and therefore distributed pressure losses limited to a few meters of service pipes, the SRO configuration should imply a submersed pipe connecting the RO unit (above the sea level) with the injection pump (at the seabed). Distributed pressure losses should be therefore not negligible in the SRO configuration and, under the hypothesis of smooth pipes and $3000 < Re < 100000$, can be estimated by Blasius correlation as:

$$\Delta p_{dist,NJ} = \frac{1}{2} f \frac{H}{d} \rho v^2, \quad (8)$$

where $v = \frac{YQ}{(\pi d^2/4)}$ is the fluid velocity, d the pipe diameter, H the pipe length (*i.e.* the seabed depth, as a first approximation), $f = \frac{0.316}{Re^{0.25}}$ the Moody friction factor, $Re = \frac{\rho v D}{\mu}$ the Reynolds number, and μ the dynamic viscosity of the fluid. These distributed pressure losses increase the power required by the injection pump in the SRO configuration (Eq. 4), being the actual pressure jump to be delivered now estimated as $\Delta p_{NJ} = p_{NJ} - (p_a + \Delta p_{HY} - \Delta p_{dist,NJ})$. Localized pressure losses, instead, should be mainly ascribed to the fluid flow within the RO units, and their value is typically provided by the membrane manufacturer ($\Delta p_{loc,RO}$). Localized pressure losses lead to decreased brine pressure and are equally present in both SRO and DSRO configurations.

In RO units, a pressure larger than p_a at the permeate side of the membrane is often encountered. However, the pressurized permeate cannot, in any circumstance, exceed the pressure on the feed side of the membrane (*i.e.* backpressure). In fact, this condition causes a reverse fluid flow through the membrane, which may lead to severe and irreversible structural damages on both envelope and active layer of the membrane. A tolerance to backpressure is typically provided by the membrane producer, but dedicated hydraulic systems (e.g., dump valves, check valves) and control should be designed in RO plants with pressurized permeate, to avoid backpressure conditions. In the DSRO concept plant, permeate pressurization would have remarkable effects on both energy performance and technical implementation of the system.

Figure 3 shows a block diagram of a DSRO plant with pressurized permeate. Three main elements of the system can be noticed: (i) a RO unit; (ii) a brine re-pressurization pump; (iii) a pump to inject permeate (distilled) water into the oilfield. In this case, a pressure regulator is not needed to decrease the feed pressure ($p_a + \Delta p_{HY}$, hydrostatic pressure at the seabed), because the pressurized permeate allows to keep supportable pressure jumps on the RO membranes. Thus, brine flows out from the RO unit with a pressure close to the external deep-sea environment (*i.e.* $p = p_a + \Delta p_{HY} - \Delta p_{loc,RO}$), being the only difference due to localized pressure losses in the RO units, and energy recovery systems are not necessary any more. The permeate side is kept pressurized thanks to the presence of a fluid column (Δp_{BP}) in the breathing tube. This fluid column also reduces the actual pressure jump to be provided by the injection pump to the permeate water, namely $\Delta p_{NJ} = p_{NJ} - (p_a + \Delta p_{BP})$. The permeate pressure must be chosen to not exceed the maxi-

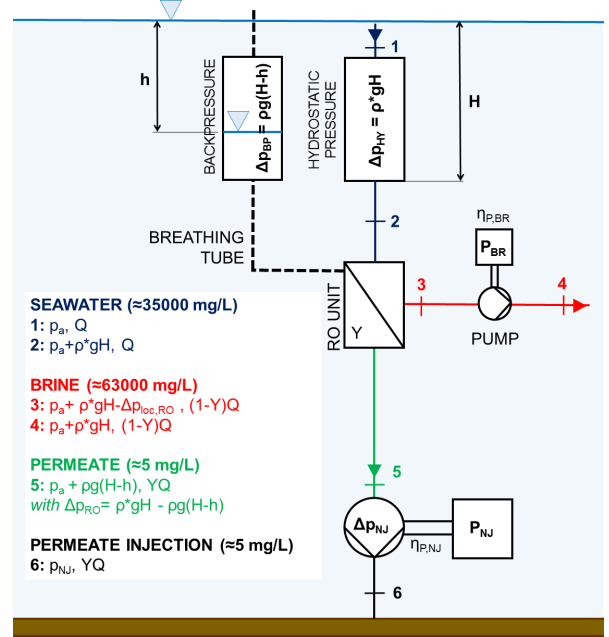


Figure 3: Schematic of a reverse osmosis plant for EOR located at the seabed (Deep-Sea Reverse Osmosis, DSRO). Hydraulic connections between elements are differently colored according to the flowing fluid: seawater (blue, TDS $\approx 35000 \text{ mg L}^{-1}$); brine (red, TDS $\approx 63000 \text{ mg L}^{-1}$); permeate water (green or black, TDS $\approx 5 \text{ mg L}^{-1}$). The black dashed line represents the breathing tube, which connects RO units with the ambient pressure. The breathing tube is filled by permeate water, to pressurize the permeate water. The inlet/outlet of each element in the schematic is numbered, with the corresponding pressure and volumetric flow of the fluid specified in the white text box at the bottom left. Note that the indicated pressures consider pressure losses.

mum operating pressure on the membrane, that is

$$\Delta p_{RO} = \Delta p_{HY} - \Delta p_{BP}. \quad (9)$$

To this purpose, while the seabed depth (H) and thus Δp_{HY} are defined by the specific installation site, Δp_{BP} can be tuned by the height ($H-h$) of the fluid column within the breathing tube, namely

$$\Delta p_{BP} = \rho g(H-h). \quad (10)$$

Hence, Eq. 9 and 10 define the maximum depth of the permeate water column in the breathing tube as:

$$h = \frac{\Delta p_{RO} - gH(\rho^* - \rho)}{\rho g}. \quad (11)$$

The total power needed by the EOR process can be again estimated by the power balance in Eq. 5, with $P_{ER} = 0$, the power required by the pump for brine re-pressurization equal to

$$P_{BR} = \frac{(1-Y)Q\Delta p_{loc,RO}}{\eta_{P,BR}}, \quad (12)$$

and the power required by injection pump (P_{NJ}) the same as Eq. 4.

3. Results

In this Section, systems for low salinity EOR made of either SRO or DSRO plants are compared from an energy point of view. Here, the aim is to identify the operating conditions determining the energy convenience of either SRO or DSRO processes under ideal or field conditions. To this purpose, a case study of DSRO plant is designed and engineered for a representative offshore installation.

3.1. Energy balance of ideal systems

The energy performance of ideal low salinity EOR systems are first analyzed. With the aim to achieve a simple analytical formulation for the energy comparison between SRO and DSRO systems, let us set the following condition:

$$H = \frac{\Delta p_{RO}}{\rho g}, \quad (13)$$

namely a seabed depth such that $\Delta p_{HY} = \Delta p_{RO}$ (see Section 3.3 for a sensitivity analysis on H , instead). The condition in Eq. 13 means that the pressure regulator and the energy recovery device (see Fig. 2) are no more required in the DSRO system. Furthermore, for the sake of simplicity, let us assume a fixed pump efficiency, namely

$$\eta_P = \eta_{P,RO} = \eta_{P,BR}. \quad (14)$$

By considering the hypotheses in Eq. 13 and 14, the net power needed by the ideal SRO process (Eqs. 1, 2, 3 and 4) becomes

$$P_{GR} = \frac{Q\Delta p_{RO}}{\eta_P} [1 - \eta_R \eta_P (1 - Y)]. \quad (15)$$

Regarding the DSRO plant, Eq. 13 and 14 imply that P_{BR} (Eq. 6) and P_{ER} (Eq. 7) are equal to zero, because brine re-pressurization is not needed and thus $P_{DS} = 0$. However, while in the SRO plant permeate water has pressure $p = p_a + \Delta p_{HY}$ at the injection pump inlet (point n. 6 in Fig. 1), in the DSRO plant the permeate pressure is only $p = p_a$ (point n. 5 in Fig. 2), because of the effect of breathing tube. Therefore, for a fair energy comparison with the SRO case, we must consider the additional pumping power that, in principle, is needed to pressurize the permeate water from DSRO plant before oilfield injection, namely $\frac{YQ\Delta p_{HY}}{\eta_P}$. By recalling the

assumption in Eq. 13, the actual net power needed by the DSRO process can be then expressed as

$$P_{DS}^* = \frac{YQ\Delta p_{RO}}{\eta_P}. \quad (16)$$

A ratio between Eq. 15 and 16 can be finally considered to evaluate the possible energy convenience of deep-sea plants:

$$\frac{P_{DS}^*}{P_{GR}} = \frac{Y}{1 - \eta_R \eta_P (1 - Y)}, \quad (17)$$

where $\frac{P_{DS}^*}{P_{GR}} \rightarrow 1$ indicates no energy convenience and $\frac{P_{DS}^*}{P_{GR}} \rightarrow 0$ significant energy convenience of DSRO configurations. It is interesting to note that: (i) in case of ideal RO membranes (no brine production, all seawater is transformed into distilled water), $Y \rightarrow 1$ and Eq. 17 tends to $\frac{P_{DS}^*}{P_{GR}} \rightarrow 1$; (ii) in case of ideal hydraulic machines, $\eta_R, \eta_P \rightarrow 1$ and Eq. 17 also tends to $\frac{P_{DS}^*}{P_{GR}} \rightarrow 1$. In other words, when ideal conditions are approached (ideal membranes, hydraulic machines, or both), the energy required by SRO or DSRO processes is the same, given the first law of thermodynamics.

In Fig. 4, the ratio in Eq. 17 is investigated for some case studies of engineering interest. On the left-hand side, Fig. 4a reports $\frac{P_{DS}^*}{P_{GR}}$ versus recovery ratios spanning from 0 to 1, being $\eta_R = 0.5, 0.7$ (Pelton turbine) or 0.9 (Francis turbine, pressure exchanger); on the right-hand side, Fig. 4b reports $\frac{P_{DS}^*}{P_{GR}}$ versus energy recovery efficiencies spanning from 0 to 1, being $Y = 0.2$ (single stage RO, seawater), 0.5 (multi stage RO, seawater) or 0.9 (multi stage RO, brackish water). In Fig. 5, instead, $\frac{P_{DS}^*}{P_{GR}}$ is plotted versus both Y and η_R to obtain a 2D energy convenience map, where the shades of blue ($\frac{P_{DS}^*}{P_{GR}} \rightarrow 0$) indicate increasing energy convenience of deep-sea RO units respect to surface ones.

Results highlight that the convenience of DSRO respect to SRO desalination for EOR increases as either membranes or hydraulic machines tend to move away from ideal conditions, namely $Y \rightarrow 0$ or $\eta_R \rightarrow 0$, with a particularly stronger sensitivity to recovery ratio (at least at fixed η_P). For example, in a desalination system designed to treat seawater with a single stage RO process and equipped with a pressure exchanger, the DSRO configuration presents 50% energy savings respect to the traditional SRO one.

3.2. Engineering of a case study

The implementation of a deep-sea reverse osmosis system may encounter some technical barriers to face,

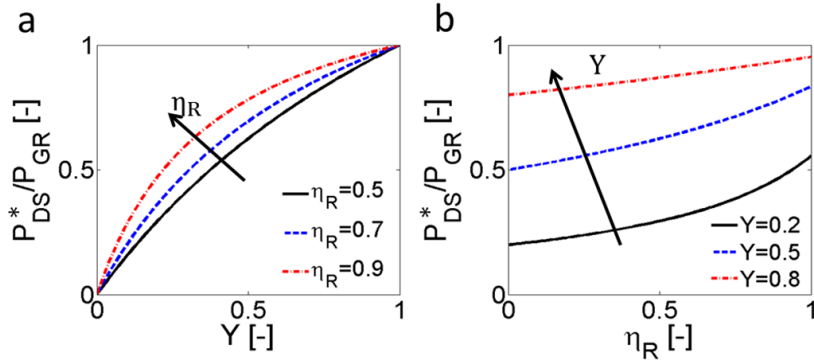


Figure 4: Energy comparison between ideal deep-sea and surface reverse osmosis units. (a) The ratio between the power needed by deep-sea and surface RO units ($\frac{P_{DS}^*}{P_{GR}}$, see Eq. 17) is plotted versus the considered recovery ratio of RO units (Y). Different curves are depicted to show the effect of the efficiency of energy recovery devices (η_R , see legend for color codes). (b) $\frac{P_{DS}^*}{P_{GR}}$ is plotted versus η_R . Different curves are plotted to evaluate the effect of Y (see legend for color codes). Note that $\eta_P=0.8$ (fixed).

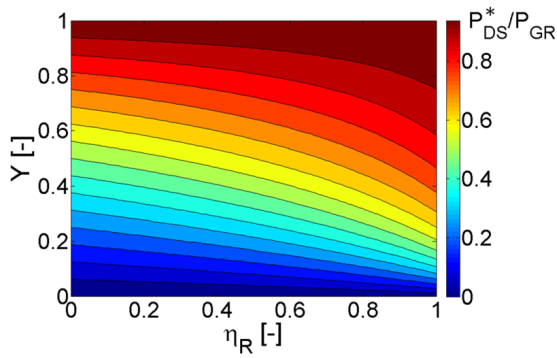


Figure 5: Energy convenience map between ideal deep-sea and surface reverse osmosis units. The ratio between the power needed by deep-sea and surface RO units ($\frac{P_{DS}^*}{P_{GR}}$, see Eq. 17 and the legend for color codes) is plotted versus the considered recovery ratio of RO units (Y) and the efficiency of energy recovery devices (η_R). Note that $\eta_P=0.8$ (fixed).

such as the undersea installation of the units, the mechanical resistance of the vessels at the seabed, the possible air entrainment issues in the injection pump, and the maintenance of the reverse osmosis modules at deep-sea. Here, a case study is designed and then preliminarily engineered to discuss the feasibility and energy performance of DSRO for low salinity EOR under realistic conditions.

As sketched in Fig. 6, a DSRO concept plant for EOR should be made of: (i) a breathing tube connecting the RO unit with a floating platform; (ii) one or more vessels containing the deep-sea RO elements (including re-pressurization pumps and energy recovery system),

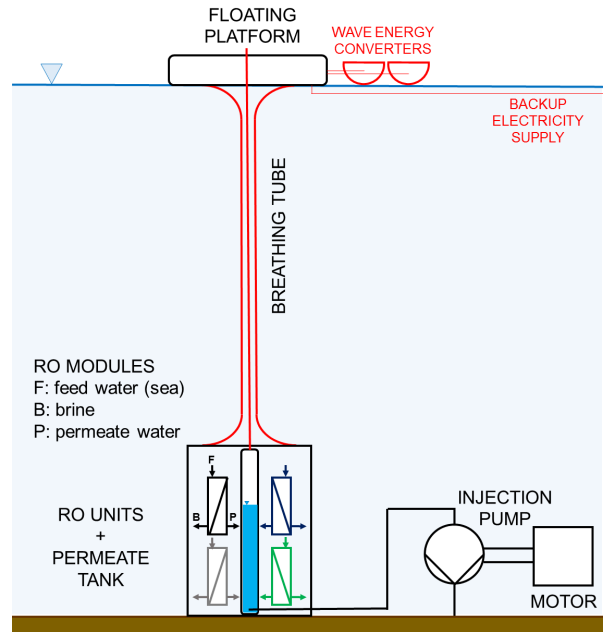


Figure 6: Case study for the enhanced oil recovery by injection of low salinity water generated by a reverse osmosis unit located at the seabed. The DSRO unit may be powered by different renewable energy sources, with the presence of a backup energy supply.

anchored to the seabed; (iii) a tank collecting the permeate; (iv) an injection pump, to pump the permeate into the oil reservoir. Furthermore, multiple renewable sources (e.g. wind turbines, wave energy converters, floating PV or marine current turbines) can contribute to power the offshore EOR unit [55], together with a conventional backup energy source to guarantee contin-

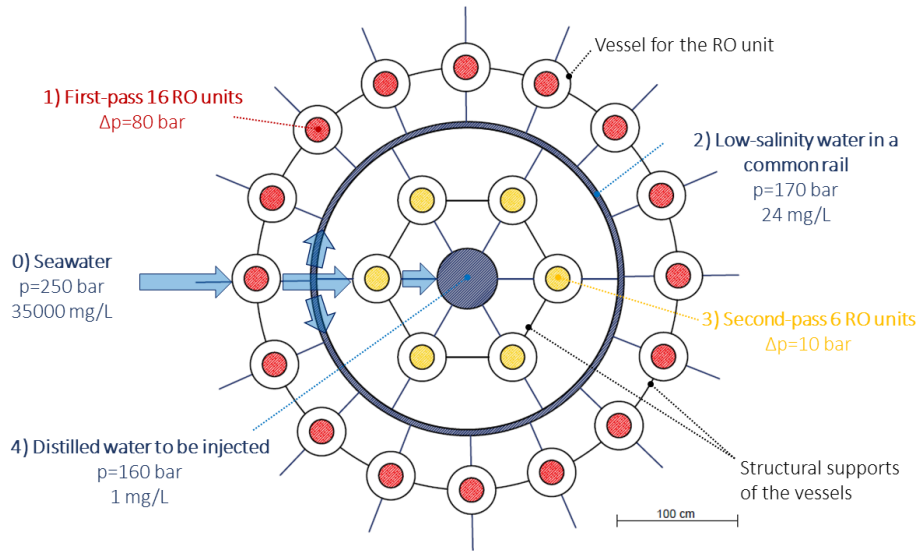


Figure 7: Technical implementation of the case study of a DSRO plant for low salinity EOR, located at approximately 2500 m below the sea level and with pressurized permeate at the outlet of RO units. Black lines represent either the vessel of RO units or their structural support. The dimension and amount of RO vessels have been sized according to the considered case study (low salinity water to be injected into the oilfield: $1000 \text{ m}^3 \text{ day}^{-1}$, see Appendix A for further details). Notice that similar solutions could be envisioned also for non-pressurized permeate.

uous operations. The installation of underwater technical systems could leverage on the broad experience of oil companies in subsea engineering [56, 57], which relies on manual or robotic submarines to assemble, operate, and maintain mechanical systems (e.g., injection pumps, safety valves, sensors, power units) while safeguarding the environment and making the exploitation of the subsea hydrocarbons economically feasible [58–60]. Notably, oil companies have also recently adopted advanced simulation and statistical tools for a preliminary virtual testing of deep-water systems, with the aim to predict in advance costly faults of subsea systems and components [61]. Furthermore, material science and engineering are continuously developing materials suitable for the harsh conditions experienced at deep-sea in terms of high pressure, low temperature, chemical and mechanical corrosion [62].

The general configuration reported in Fig. 6 is then engineered in accordance with typical operating conditions for offshore oilfields. In detail, the RO plant is sized to provide a volumetric flow of low salinity permeate equal to $YQ = 1000 \text{ m}^3 \text{ day}^{-1}$. The inlet seawater considered in this case study has $\text{TDS} \approx 35000 \text{ mg L}^{-1}$ ($\text{pH} = 7.6$) and must be desalted to lower salinity values, eventually less than 5 mg L^{-1} . Starting from these design requirements, the amount, size, and type of RO elements is defined by considering off-the-shelf products (see Tab. A1 for details).

The identified amount and size of RO elements can be used to determine the diameter and height of the submerged vessels, which should contain these RO units and the permeate tank. Structural and buckling resistance criteria are then adopted to calculate the minimum thickness of these vessels at the seabed, considering an extreme depth of 2500 m. The DSRO concept plant in Fig. 7 is proposed – for example – to implement the considered case study with pressurized permeate, since splitting the RO elements into multiple small submerged vessels (each one with pressurized permeate) mitigates possible structural and buckling issues (see Appendix A for a preliminary structural verification). In detail, seawater (250 bar, 35000 mg L^{-1}) is processed by (1) a first-pass reverse osmosis process (16 vessels containing the RO elements; pressure drop at the membrane: 80 bar), which produces (2) low salinity water (170 bar, 24 mg L^{-1}). Low salinity water is then collected by a common rail and processed by (3) a second-pass reverse osmosis process (6 vessels containing the RO elements; pressure drop at the membrane: 10 bar), which produces distilled water (160 bar, $\sim 1 \text{ mg L}^{-1}$). Finally, distilled water is accumulated in a vessel and then injected into the oilfield. Note that the presence of a water column at the permeate side avoids possible problems of air entrapment, which may damage the injection pump.

	Y[-]	H [m]	YQ [m ³ day ⁻¹]	η_R [-]
Lower	0.1	850	500	0.6
Upper	1	2400	1500	0.95

Table 1: Lower and upper limits of the variables explored in the sensitivity analysis comparing SRO and DSRO energy performances.

3.3. Sensitivity analyses on the case study

The case study discussed in Section 3.2 is then used to perform sensitivity analyses on the most influencing parameters affecting the energy performances of SRO and DSRO plants for EOR. In detail, the variables explored in four different sensitivity analyses are:

- Y, recovery ratio of the RO unit;
- YQ, volumetric flow rate of the low salinity water to be injected in the offshore oilfield;
- H, seabed depth;
- η_R , efficiency of the energy recovery device (if present).

Starting from a base case, the values of these variables are progressively changed to assess the sensitivity of the ratio between DSRO and SRO net power needs ($\frac{P_{L,DS}}{P_{L,GR}}$). As a base case, the following values are adopted: Y = 0.2 (seawater, single passage in the RO unit); YQ = 1000 m³ day⁻¹ (representative EOR needs for offshore oilfields); H = 1000 m (representative seabed depth for offshore oilfields); $\eta_R = 0.9$ (Francis turbine). The explored intervals of the variables, instead, are determined by values of engineering interest (see Tab. 1). For example, while YQ and H depend on the installation site, Y depends on the water salinity (the lower it is, the larger Y can be attained) and on the selected RO membranes, and η_R is defined by the installed hydraulic machine (from Pelton turbine, $\eta_R = 0.8$, to pressure exchanger, $\eta_R = 0.95$).

Some variables are not explored in the sensitivity analyses because of their negligible impact on the energy comparison between SRO and DSRO systems, and their considered values are: $\eta_{P,RO} = \eta_{P,BR} = \eta_{P,NJ} = 0.8$ the efficiency of the pumps in the reverse osmosis, brine re-pressurization and injection processes, respectively; $\Delta p_{RO} = 82$ bar the pressure jump across the RO membrane, which is defined by the maximum operating conditions supportable by the selected membranes (Dow Filmtech™ SW30XHR-440i); $p_{NJ} = 300$ bar the requested injection pressure in the oilfield; d = 0.2 m the diameter of the submersed pipe between RO and injection units. Distributed pressure losses in SRO

plants are estimated by Eq. 8, with resulting values in the $\Delta p_{dist,NJ} \approx 0.07$ – 0.17 bar range; localized pressure losses due to RO units are provided by Dow for Filmtech™ SW30XHR-440i as $\Delta p_{loc,RO} \approx 2$ bar. Furthermore, the considered constants are: $g = 9.81$ m s⁻² the gravitational acceleration; $\rho = 1000$ kg m⁻³ the water density; $\rho^* = 1030$ kg m⁻³ the seawater density; $p_a = 1$ bar the ambient pressure; $\mu = 1.307 \times 10^{-3}$ Pa s the dynamic viscosity of water at an average temperature of 283 K.

Three scenarios of SRO and DSRO plants are considered in the sensitivity analyses, namely:

- Scenario 1: ideal conditions (*i.e.* no pressure losses) for both plants.
- Scenario 2: distributed and localized pressure losses for both plants.
- Scenario 3: distributed and localized pressure losses for both plants, and a pressurized permeate in the DSRO plant.

In each scenario, the power balance for both SRO and DSRO plants is fully computed in the different sensitivity analyses and, finally, the $\frac{P_{L,DS}}{P_{L,GR}}$ ratio calculated. Table 2 summarizes the equations considered in the three scenarios, as previously described in Section 2.

As a reference, the base case (Y = 0.2, YQ = 1000 m³ day⁻¹, H = 1000 m, and $\eta_R = 0.9$) in the Scenario 1 shows $P_{L,DS} = 443$ kW, $P_{L,GR} = 543$ kW, and thus $\frac{P_{L,DS}}{P_{L,GR}} = 0.82$, namely a potential 18% energy convenience of the deep-sea solution respect to the surface one. Clearly, a reduced electrical power requirement for a given configuration would lead to lower energy costs of DSRO than SRO during EOR operations, which should balance the prospected higher installation and maintenance costs instead. The full picture of the four sensitivity studies in the three different scenarios is presented in Fig. 8. In detail, the trend of $\frac{P_{L,DS}}{P_{L,GR}}$ is plotted versus the recovery ratio (Fig. 8a), the volumetric flow of permeate water injected into the oilfield (Fig. 8b), the seabed depth (Fig. 8c), and the efficiency of energy recovery devices (Fig. 8d).

Results show that DSRO is generally energy convenient respect to SRO in EOR applications ($\frac{P_{L,DS}}{P_{L,GR}} < 1$), and up to 50% energy savings can be eventually obtained. As already noticed in case of ideal systems (Section 3.1), better energy conveniences of DSRO plants are achieved with lower Y and η_R values, namely with membranes and hydraulic machines far from ideal conditions. While η_R has only a moderate effect on $\frac{P_{L,DS}}{P_{L,GR}}$ (up

		Scenario 1	Scenario 2	Scenario 3
Surface RO	P_{RO}	$\frac{Q\Delta p_{RO}}{\eta_{P,RO}}$	same as Scenario 1	same as Scenario 1
	P_{ER}	$\eta_R(1-Y)Q\Delta p_{RO}$	$\eta_R(1-Y)Q(\Delta p_{RO} - \Delta p_{loc,RO})$	same as Scenario 2
	P_{NJ}	$\frac{Y(Q\Delta p_{NJ})}{\eta_{P,NJ}}$, being: $\Delta p_{NJ} = p_{NJ} - (\rho gH + p_a)$	$\frac{Y(Q\Delta p_{NJ})}{\eta_{P,NJ}}$, being: $\Delta p_{NJ} = p_{NJ} - (\rho gH + p_a - \Delta p_{dist,NJ})$	same as Scenario 2
Deep-sea RO	P_{BR}	$\frac{(1-Y)Q(\rho^*gH - \Delta p_{RO})}{\eta_{P,BR}}$	$\frac{(1-Y)Q(\rho^*gH - \Delta p_{RO} + \Delta p_{loc,RO})}{\eta_{P,BR}}$	$\frac{(1-Y)Q\Delta p_{loc,RO}}{\eta_{P,BR}}$
	P_{ER}	$\eta_R Q(\rho^*gH - \Delta p_{RO})$	same as Scenario 1	0
	P_{NJ}	$\frac{Y(Q\Delta p_{NJ})}{\eta_{P,NJ}}$, being: $\Delta p_{NJ} = p_{NJ} - p_a$	same as Scenario 1	$\frac{Y(Q\Delta p_{NJ})}{\eta_{P,NJ}}$, being: $\Delta p_{NJ} = p_{NJ} - [\rho g(H - h) + p_a]$

Table 2: Equations adopted in the sensitivity analyses comparing surface and deep-sea RO energy performance. Note that P_{RO} is the power required to pressurize seawater at the inlet of RO units, P_{ER} the power generated by energy recovery devices, P_{NJ} the power required to inject distilled water into the oilfield, and P_{BR} the power required to re-pressurize brine at the outlet of RO units. Moreover, Scenario 1 refers to ideal conditions of RO plants; whereas Scenario 2 considers pressure losses and Scenario 3 pressure losses and a pressurized permeate in the RO units of the DSRO plant.

to 25% in the considered η_R range), the positive effect of Y on DSRO performance has a larger magnitude (up to 67% in the considered Y range). In fact, a lower Y implies higher inlet volumetric flows to be pressurized (and thus pumping power) in the SRO plant, at fixed amount of produced distilled water. Distributed and localized pressure losses, instead, show only a marginal impact on power balances (typically less than 2%); whereas the requested volumetric flow rate of low salinity water into the oilfield shows no effects at all. Finally, the permeate pressurization has a general positive impact (up to 60%) on the energy convenience of DSRO in all the sensitivity studies and scenarios, due to the reduced power needed for distilled water injection into the oilfield. This is particularly relevant for hydrostatic pressures larger than the maximum reverse osmosis pressure (*i.e.* above ≈ 800 m), because DSRO configurations without pressurized permeate largely dissipate the potential energy in the hydrostatic pressure of inlet seawater, while the fluid column of permeate in the submersed pipe of SRO is fully exploited to reduce the power needs of the injection pump.

3.4. 3D maps for quick design

For the sake of completeness and based on the detailed analysis presented in Section 3.3, we finally pro-

pose a compact representation that readily allows to evaluate the convenience of deep-sea RO with respect to the surface one for EOR application. To this purpose, we introduce the gain coefficient as $G = 1 - \frac{P_{LDS}}{P_{LGR}}$, and then plot it as a function of the two more affecting parameters, namely Y and H . Notice that, since the ratio $\frac{P_{LDS}}{P_{LGR}}$ reported in Fig. 8b and Fig. 8d does not vary significantly with the volumetric flow of permeate water injected into the oilfield (YQ) and the efficiency of the recovery device (η_R), their effect has not been investigated again here.

Results are reported in Fig. 9: the map on the left-hand side of Fig. 9 refers to Scenario 2, whilst the one reported on the right-hand side to Scenario 3. In the Scenario 3, considering the ranges of H and Y reported in Table 1, a deep-sea reverse osmosis unit is always more energy convenient respect to the surface one, allowing to save up to about 60% of energy. Instead, the area of the map labeled in light pink reported on the left-hand side of Fig. 9 represents the configurations for which the surface RO unit is still energetically convenient in the Scenario 2.

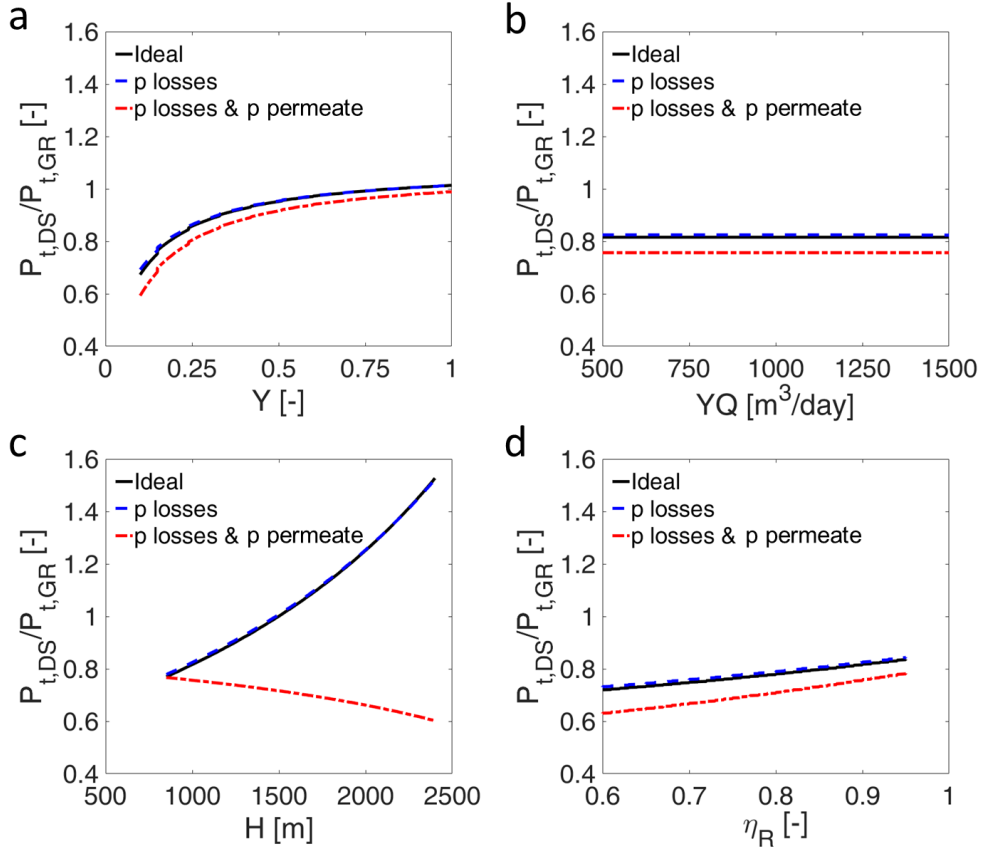


Figure 8: Energy comparison between deep-sea and surface reverse osmosis units. (a) The ratio between the total power needed by deep-sea and surface RO units for EOR application ($\frac{P_{t,DS}}{P_{t,GR}}$) is plotted versus the considered recovery ratio of RO units (Y), (b) volumetric flow of permeate water injected into the oilfield (YQ), (c) seabed depth (H), and (d) efficiency of energy recovery devices (η_R). Colored curves are plotted to compare different scenarios: ideal RO units (Scenario 1, black solid lines); RO units with distributed and localized pressure losses (Scenario 2, blue dashed lines); RO units with distributed and localized pressure losses, and pressurized permeate in the deep-sea RO plant (Scenario 3, red dash-dot lines).

4. Conclusions

Enhanced oil recovery (EOR) by low salinity water injection into oilfields has demonstrated to effectively enhance the efficiency of crude oil extraction. However, energy costs related to the production of low salinity water, typically by reverse osmosis (RO) desalination, should be reduced to achieve a more sustainable EOR process.

In this article, a novel strategy for low salinity water production particularly suited for offshore applications is discussed. In particular, the operation of reverse osmosis units anchored at the seabed is demonstrated to be generally more energy convenient than traditional plants installed above the sea level. To our best knowledge, in this study we demonstrate for the first time that DSRO can be more advantageous from the energy perspective than the more traditional SRO. In this respect,

the first key finding of this study consists in the assessment of the origin of energy consumption disparity between DSRO and SRO arising from non-ideality processes of reverse osmosis and hydraulic machines. This has been quantified by introducing a proper power ratio that is capable to compare the two different approaches. An additional key finding of this work consists in the first preliminary sizing of a DSRO, where critical dimensions, materials and operating conditions have been reported for a system intended to produce 1000 m^3 per day. To this end, sensitivity analyses on a realistic case allow to explore the most important variables determining the energy convenience of DSRO respect to surface RO plants (up to 50% energy savings). A particularly original result is the quantification of the positive effect of pressurized permeate on the DSRO performances. Other effects, such as pressure losses, different salinity/temperature of inlet seawater, or permeate volumet-

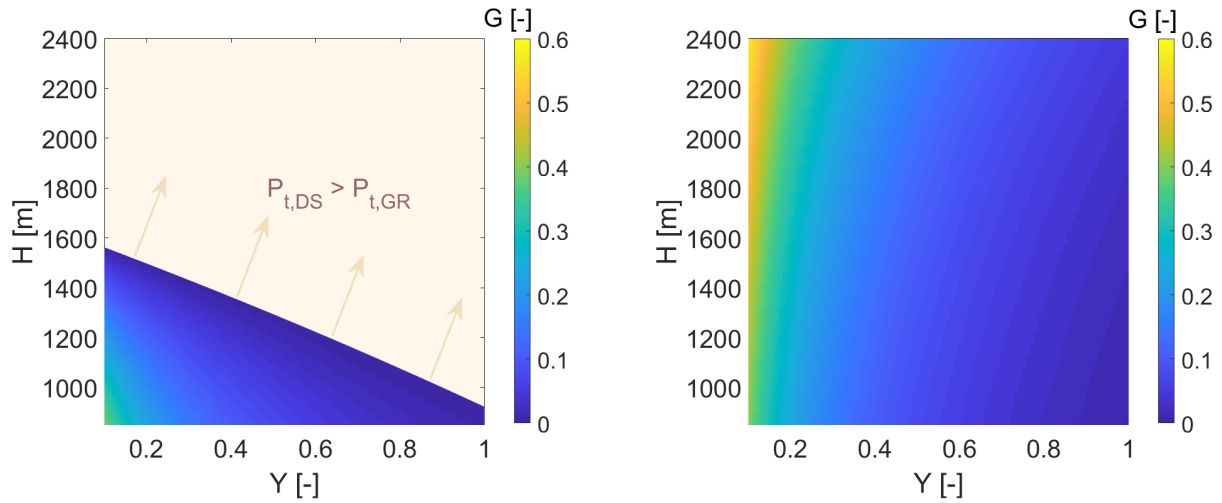


Figure 9: The gain term $G = 1 - \frac{P_{t,DS}}{P_{t,GR}}$ is plotted as function of Y and H . The maps on the left-hand side and right-hand side are referred to Scenario 2 and 3, respectively. The volumetric flow of permeate water injected into the oilfield (YQ) is kept constant and equal to $1000 \text{ m}^3 \text{ day}^{-1}$, whilst the efficiency of energy recovery devices (η_R) is equal to 0.9.

ric flow have only a minor impact on the overall energy balances and thus can be safely neglected.

In perspective, because of the reduced energy needs, the proposed DSRO solution for low salinity EOR may be eventually powered by renewable sources only, namely through the exploitation of sea waves or underwater currents. A further advantage of deep-sea RO is the reduced pressure oscillation at the membrane inlet, which slows down the membrane degradation.

Currently, the major technical open issues related to DSRO plants are: the implementation of hydraulic and control systems capable to handle a (deep-sea) pressurized permeate and to avoid possible backpressure damages on the membrane; the definition of a reliable and inexpensive maintenance strategy for the submersed RO units (see Appendix B for some discussions); the engineering of deep-sea vessels containing both RO units and permeate tank, with special focus on preventing buckling issues. Finally, the potential energy convenience of deep-sea desalination plants is not sufficient to guarantee the actual feasibility of this EOR solution: both an economic analysis on capital and operating costs of SRO and DSRO plants, and a broader cost-benefit analysis of low salinity EOR respect to other EOR techniques should be considered as well in future studies.

Acknowledgments

This work was supported by ENI S.p.A. This article is published online at <https://doi.org/10.1016/j.apenergy.2021.117661>.

apenergy.2021.117661.

Appendix A. Sizing the case study of low salinity EOR

The case study considered for the process of enhanced oil recovery by low salinity water injection takes inspiration from the typical operating conditions for offshore oilfields. In detail, the RO plant is sized to provide a volumetric flow of low salinity permeate equal to $YQ = 1000 \text{ m}^3 \text{ day}^{-1}$, at a typical seabed depth of 2500 m. The considered inlet seawater has $\text{TDS} \approx 35000 \text{ mg L}^{-1}$ ($\text{pH} = 7.6$) and must be desalted to lower salinity values, eventually less than 5 mg L^{-1} .

The design of this case study is based on off-the-shelf Dow[®] RO elements, by means of ROSA (Reverse Osmosis System Analysis) software. The sizing has been done with the target to minimize the plant dimensions (*i.e.*, number of RO elements) and thus operating at the highest pressure allowed by the Dow's reverse osmosis element currently present on the market, namely 83 bar. This is due to the cost involved in deep-sea RO: while installation and maintenance costs are directly proportional to plant dimensions, energy costs are independent from RO pressure, being the desalination process driven by the sole hydrostatic pressure at the seabed [63].

As detailed in Tab. A1, the results of the design process show that two successive RO passes are needed to achieve water salinities below 5 mg L^{-1} . The first pass allows to reduce seawater salinity from 35000 mg L^{-1} to 24 mg L^{-1} (*i.e.* low salinity water); the second pass

	I Pass	II Pass
n. pressure vessels	16	6
n. elements per vessel	5	4
Feed flow [m ³ day ⁻¹]	4444	1626
Permeate flow [m ³ day ⁻¹]	1626	1000
Permeate TDS [mg L ⁻¹]	24	0.6
Feed pressure [bar]	83	15
Brine pressure [bar]	81	14

Table A1: Design of the RO units for the considered case study (required permeate flow: 1000 m³ day⁻¹). Note that the difference between feed and brine pressures is given by the localized pressure losses in the RO elements.

from 24 mg L⁻¹ to 0.6 mg L⁻¹ (*i.e.* distilled water), which may be unnecessary in case of low salinity EOR. Note that the second RO pass (and its pumps) could be also avoided by introducing more compact ion exchangers, which should be periodically substituted. The first pass can be performed in 16 pressure vessels (with 5 RO elements each); whereas the second pass in 6 pressure vessels (with 6 RO elements each). In particular, Dow Filmtech™ SW30XHR-440i RO elements are considered for the first pass (41 m²/each active area; 1029 mm length and 201 mm diameter); while Dow Filmtech™ XLE-440 for the second pass (41 m²/each active area; 1016 mm length and 201 mm diameter).

For a preliminary feasibility analysis, both structural and buckling resistance of the submerged vessels in the concept DSRO plant in Fig. 7 are assessed. First, the structural resistance of the vessels is tested by Tresca criterion for containers subjected to an external pressure (Δp):

$$s \geq \frac{1}{2} \frac{\Delta p D}{\sigma_{adm}}, \quad (A1)$$

being σ_{adm} the admissible stress and s the vessel thickness. By assuming a yield strength equal to $\sigma_y = 600$ MPa (stainless steel), the admissible stress on the vessels can be obtained from the safety factor as $\sigma_{adm} = \frac{5}{8} \sigma_y = 375$ MPa. Note that these results are also valid if Von Mises criterion is adopted instead, because of its less stringent constraint. Second, the resistance of these submerged vessels to buckling is also verified. To this purpose, the condition to be guaranteed in case of cylindrical vessels subjected to external pressure is:

$$\Delta p < \frac{2E}{3} \left(\frac{s}{D} \right)^3, \quad (A2)$$

where E is the Young's modulus of the vessel ($E=200$ GPa for stainless steel).

In general, better pressure and buckling resistance can be achieved by splitting the RO elements into multiple smaller vessels, each one with a pressurized permeate. Given the diameter of the selected filtration elements (about 20 cm each) in the concept design depicted in Fig. 7, we have verified the mechanical resistance of submersed stainless-steel vessels with 40 cm diameter and pressurized permeate at the extreme seabed depth of 2500 m. Both Tresca and buckling criteria are verified for $s \geq 1.6$ cm (first-pass units) and $s \geq 1.7$ cm (second-pass units), thus showing the feasibility of the considered case study of DSRO system. Similarly, the produced low salinity water could be stored in an injection vessel with 50 cm diameter and at least 2.1 cm thickness. Since the limiting sizing criterion is the buckling one, thinner vessels could be obtained – for instance – by adding ribs and/or several cylindrical shells to reinforce the vessels.

Appendix B. Maintenance of DSRO plants

Reverse osmosis membranes are typically subject to scaling and fouling events, which decrease their productivity. Both scaling and fouling processes can be slowed down by pretreating inlet seawater: while scaling is minimized by chemical or ion exchange techniques, fouling is reduced by either mechanical processes (removal of suspended solids) or chemical treatments (fouling deactivation). These pretreatments should be introduced also in DSRO plants, to enhance the durability of RO membranes for EOR applications [64].

Membrane fouling can be reversed by periodical low pressure cleaning with (1) appropriate chemicals and (2) permeate water, preferably at $T > 20$ °C. Therefore, in a deep-sea RO plant, the amount of RO units should be oversized, in order to allow the maintenance of its elements on a rotation basis. In this way, a service ship could periodically approach the floating platform and then inject the cleaning chemicals into the RO units under maintenance by means of an *ad hoc* flexible pipe close to (or inside) the riser (see Fig. A1), without compromising the continuous operation of EOR process. Besides such regular maintenance of membranes operated by service ships, extraordinary maintenance, repairs or simple inspection of the subsea components can be carried out by manned or unmanned underwater vehicles, as routinely done in offshore oil rigs [65–67].

References

- [1] H. Hosseinzade Khanamiri, I. Baltzersen Enge, M. Nourani, J. Å. Stensen, O. Torsæter, N. Hadia, Eor by low salinity water and surfactant at low concentration: impact of injection and

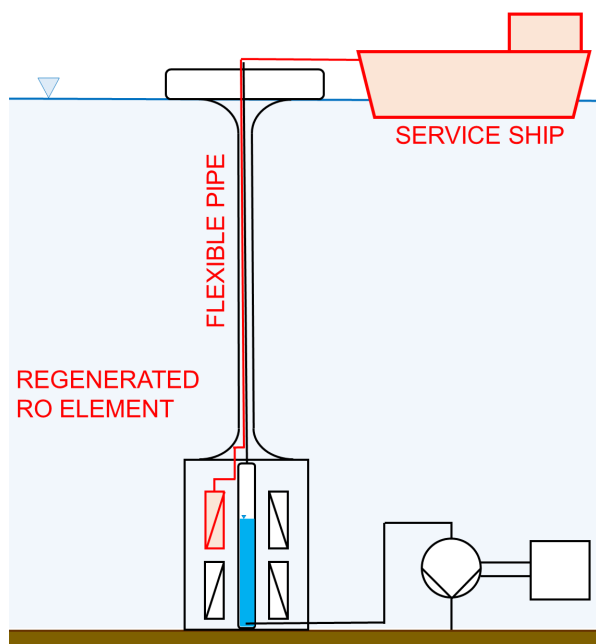


Figure A1: Schematic of the maintenance procedures of the reverse osmosis elements in a DSRO concept plant.

- in situ brine composition, *Energy & Fuels* 30 (4) (2016) 2705–2713.
- [2] E. W. Al-Shalabi, K. Sepehrnoori, A comprehensive review of low salinity/engineered water injections and their applications in sandstone and carbonate rocks, *Journal of Petroleum Science and Engineering* 139 (2016) 137–161.
 - [3] T. Austad, A. RezaeiDoust, T. Puntervold, et al., Chemical mechanism of low salinity water flooding in sandstone reservoirs, in: *SPE improved oil recovery symposium*, Society of Petroleum Engineers, 2010.
 - [4] V. Alvarado, E. Manrique, Enhanced oil recovery: an update review, *Energies* 3 (9) (2010) 1529–1575.
 - [5] T. Ebrahim, V. S. Mohsen, S. M. Mahdi, K. T. Esmacel, A. Saeb, Performance of low-salinity water flooding for enhanced oil recovery improved by sio 2 nanoparticles, *Petroleum Science* 16 (2) (2019) 357–365.
 - [6] B. Zhang, A. I. Mohamed, L. Goual, M. Piri, Pore-scale experimental investigation of oil recovery enhancement in oil-wet carbonates using carbonaceous nanofluids, *Scientific reports* 10 (1) (2020) 1–16.
 - [7] L. C. Uren, E. Fahmy, et al., Factors influencing the recovery of petroleum from unconsolidated sands by waterflooding, *Transactions of the AIME* 77 (01) (1927) 318–335.
 - [8] A. I. Mohamed, A. S. Sultan, I. A. Hussein, G. A. Al-Muntasheri, Influence of surfactant structure on the stability of water-in-oil emulsions under high-temperature high-salinity conditions, *Journal of Chemistry* 2017 (2017).
 - [9] Y. Bai, C. Xiong, X. Shang, Y. Xin, Experimental study on ethanolamine/surfactant flooding for enhanced oil recovery, *Energy & fuels* 28 (3) (2014) 1829–1837.
 - [10] G. J. Hirasaki, C. A. Miller, M. Puerto, et al., Recent advances in surfactant eor, in: *SPE Annual Technical Conference and Exhibition*, Society of Petroleum Engineers, 2008.
 - [11] J. Sun, L. Sun, W. Liu, X. Liu, X. Li, Q. Shen, Alkaline con-

- sorption mechanisms by crude oil: A comparison of sodium carbonate and sodium hydroxide, *Colloids and Surfaces A: Physicochemical and Engineering Aspects* 315 (1-3) (2008) 38–43.
- [12] J. Ge, A. Feng, G. Zhang, P. Jiang, H. Pei, R. Li, X. Fu, Study of the factors influencing alkaline flooding in heavy-oil reservoirs, *Energy & fuels* 26 (5) (2012) 2875–2882.
 - [13] X. Sun, Y. Zhang, G. Chen, Z. Gai, Application of nanoparticles in enhanced oil recovery: a critical review of recent progress, *Energies* 10 (3) (2017) 345.
 - [14] A. Matteo, M. Matteo, B. Luca, F. Matteo, L. Luca, H. Gabriele, E. Sani, P. Matteo, C. Eliodoro, A. Pietro, Coffee-based colloids for direct solar absorption, *Scientific Reports (Nature Publisher Group)* 9 (1) (2019).
 - [15] T. Pak, N. L. Archilha, I. F. Mantovani, A. C. Moreira, I. B. Butler, The dynamics of nanoparticle-enhanced fluid displacement in porous media—a pore-scale study, *Scientific reports* 8 (1) (2018) 1–10.
 - [16] N. Ogolo, O. Olafuyi, M. Onyekonwu, et al., Enhanced oil recovery using nanoparticles, in: *SPE Saudi Arabia section technical symposium and exhibition*, Society of Petroleum Engineers, 2012.
 - [17] T. Tosco, M. P. Papini, C. C. Viggi, R. Sethi, Nanoscale zevalent iron particles for groundwater remediation: a review, *Journal of cleaner production* 77 (2014) 10–21.
 - [18] W.-x. Zhang, D. W. Elliott, Applications of iron nanoparticles for groundwater remediation, *Remediation Journal: The Journal of Environmental Cleanup Costs, Technologies & Techniques* 16 (2) (2006) 7–21.
 - [19] H. Zhang, A. Nikolov, D. Wasan, Enhanced oil recovery (eor) using nanoparticle dispersions: underlying mechanism and imbibition experiments, *Energy & Fuels* 28 (5) (2014) 3002–3009.
 - [20] B. A. Suleimanov, F. Ismailov, E. Veliyev, Nanofluid for enhanced oil recovery, *Journal of Petroleum Science and Engineering* 78 (2) (2011) 431–437.
 - [21] L. Hendraningrat, S. Li, O. Torsæter, A coreflood investigation of nanofluid enhanced oil recovery, *Journal of Petroleum Science and Engineering* 111 (2013) 128–138.
 - [22] R. T. Armstrong, S. Berg, Interfacial velocities and capillary pressure gradients during haines jumps, *Physical Review E* 88 (4) (2013) 043010.
 - [23] K. Singh, H. Menke, M. Andrew, Q. Lin, C. Rau, M. J. Blunt, B. Bijeljic, Dynamics of snap-off and pore-filling events during two-phase fluid flow in permeable media, *Scientific reports* 7 (1) (2017) 1–13.
 - [24] S. U. Pickering, Cxcvii.—emulsions, *Journal of the Chemical Society, Transactions* 91 (1907) 2001–2021.
 - [25] Y. Yang, Z. Fang, X. Chen, W. Zhang, Y. Xie, Y. Chen, Z. Liu, W. Yuan, An overview of pickering emulsions: solid-particle materials, classification, morphology, and applications, *Frontiers in pharmacology* 8 (2017) 287.
 - [26] N. S. Ahmed, A. M. Nassar, N. N. Zaki, H. K. Gharieb, Formation of fluid heavy oil-in-water emulsions for pipeline transportation, *Fuel* 78 (5) (1999) 593–600.
 - [27] T. Pak, I. B. Butler, S. Geiger, M. I. van Dijke, Z. Jiang, R. Surmas, Multiscale pore-network representation of heterogeneous carbonate rocks, *Water Resources Research* 52 (7) (2016) 5433–5441.
 - [28] R. Aziz, V. Joekar-Niasar, P. J. Martínez-Ferrer, O. E. Godinez-Brizuela, C. Theodoropoulos, H. Mahani, Novel insights into pore-scale dynamics of wettability alteration during low salinity waterflooding, *Scientific reports* 9 (1) (2019) 1–13.
 - [29] A. Lager, K. J. Webb, I. R. Collins, D. M. Richmond, et al., Losal enhanced oil recovery: Evidence of enhanced oil recovery at the reservoir scale, in: *SPE symposium on improved oil*

- recovery, Society of Petroleum Engineers, 2008.
- [30] P. De Angelis, M. Tuninetti, L. Bergamasco, L. Caliano, P. Asinari, F. Laio, M. Fasano, Data-driven appraisal of renewable energy potentials for sustainable freshwater production in africa, *Renewable and Sustainable Energy Reviews* 149 (2021) 111414.
- [31] B. Ghorbani, R. Shirmohammadi, M. Amidpour, F. Inzoli, M. Rocco, Design and thermoeconomic analysis of a multi-effect desalination unit equipped with a cryogenic refrigeration system, *Energy Conversion and Management* 202 (2019) 112208.
- [32] M. Morciano, M. Fasano, L. Bergamasco, A. Albiero, M. L. Curzio, P. Asinari, E. Chiavazzo, Sustainable freshwater production using passive membrane distillation and waste heat recovery from portable generator sets, *Applied Energy* 258 (2020) 114086.
- [33] E. Chiavazzo, M. Morciano, F. Viglino, M. Fasano, P. Asinari, Passive solar high-yield seawater desalination by modular and low-cost distillation, *Nature Sustainability* 1 (12) (2018) 763–772.
- [34] F. Signorato, M. Morciano, L. Bergamasco, M. Fasano, P. Asinari, Exergy analysis of solar desalination systems based on passive multi-effect membrane distillation, *Energy Reports* 6 (2020) 445–454.
- [35] M. Morciano, M. Fasano, S. V. Boriskina, E. Chiavazzo, P. Asinari, Solar passive distiller with high productivity and marangoni effect-driven salt rejection, *Energy & Environmental Science* 13 (10) (2020) 3646–3655.
- [36] M. Elimelech, W. A. Phillip, The future of seawater desalination: energy, technology, and the environment, *science* 333 (6043) (2011) 712–717.
- [37] M. Fasano, T. Humplik, A. Bevilacqua, M. Tsapatsis, E. Chiavazzo, E. N. Wang, P. Asinari, Interplay between hydrophilicity and surface barriers on water transport in zeolite membranes, *Nature communications* 7 (1) (2016) 1–8.
- [38] M. Fasano, A. Bevilacqua, E. Chiavazzo, T. Humplik, P. Asinari, Mechanistic correlation between water infiltration and framework hydrophilicity in mfi zeolites, *Scientific reports* 9 (1) (2019) 1–12.
- [39] N. Voutchkov, Energy use for membrane seawater desalination—current status and trends, *Desalination* 431 (2018) 2–14.
- [40] E. Jones, M. Qadir, M. T. van Vliet, V. Smakhtin, S.-m. Kang, The state of desalination and brine production: A global outlook, *Science of the Total Environment* 657 (2019) 1343–1356.
- [41] G. Tang, N. R. Morrow, et al., Salinity, temperature, oil composition, and oil recovery by waterflooding, *SPE Reservoir Engineering* 12 (04) (1997) 269–276.
- [42] E. V. Lebedeva, A. Fogden, Micro-ct and wettability analysis of oil recovery from sand packs and the effect of waterflood salinity and kaolinite, *Energy & Fuels* 25 (12) (2011) 5683–5694.
- [43] K. Webb, A. Lager, C. Black, Comparison of high/low salinity water/oil relative permeability, in: *International symposium of the society of core analysts, Abu Dhabi, UAE, Vol. 29, 2008*.
- [44] S. Shaddel, S. A. Tabatabae-Nejad, S. J. Fathi, Low-salinity water flooding: Evaluating the effect of salinity on oil and water relative permeability, wettability, and oil recovery, *Special Topics & Reviews in Porous Media: An International Journal* 5 (2) (2014).
- [45] A. Lager, K. J. Webb, C. Black, M. Singleton, K. S. Sorbie, et al., Low salinity oil recovery—an experimental investigation1, *Petrophysics* 49 (01) (2008).
- [46] W.-B. Bartels, H. Mahani, S. Berg, R. Menezes, J. A. van der Hoeven, A. Fadili, et al., Oil configuration under high-salinity and low-salinity conditions at pore scale: a parametric investigation by use of a single-channel micromodel, *Spe Journal* 22 (05) (2017) 1–362.
- [47] V. Ahmetgareev, A. Zeinijahromi, A. Badalyan, R. Khisamov, P. Bedrikovetsky, Analysis of low salinity waterflooding in bastyrykskoye field, *Petroleum Science and Technology* 33 (5) (2015) 561–570.
- [48] S. Shaddel, M. Hemmati, E. Zamanian, N. N. Moharrami, Core flood studies to evaluate efficiency of oil recovery by low salinity water flooding as a secondary recovery process, *Journal of Petroleum Science and Technology* 4 (1) (2014) 47–56.
- [49] A. Janson, D. Dardor, M. Al Maas, J. Minier-Matar, A. Abdel-Wahab, S. Adham, Pressure-retarded osmosis for enhanced oil recovery, *Desalination* 491 (2020) 114568.
- [50] Y. Cui, Q. Ma, Z. Wu, H. Lu, Z. Gao, J. Fan, A hydrostatic pressure-driven desalination system for large-scale deep sea space station, *International Journal of Chemical Engineering* 2021 (2021).
- [51] P. Pacenti, M. Reali, N. Brambilla, A. Elli, P. Helm, R. Janssen, D. Chiamonti, S. Gärtner, Deployment of a submarine reverse osmosis desalination prototype plant (rodss): field tests and preliminary technical evaluations, *Desalination* 138 (1-3) (2001) 181.
- [52] C. Charcosset, C. Falconet, M. Combe, Hydrostatic pressure plants for desalination via reverse osmosis, *Renewable energy* 34 (12) (2009) 2878–2882.
- [53] D. Colombo, M. De Gerloni, M. Reali, An energy-efficient submarine desalination plant, *Desalination* 122 (2-3) (1999) 171–176.
- [54] S. Memon, Y.-D. Kim, S. Soomro, M. I. Soomro, W.-S. Kim, A new approach for freshwater production and energy recovery from an oil field, *Journal of Water Process Engineering* 34 (2020) 101145.
- [55] F. Calise, F. L. Cappiello, R. Vanoli, M. Vicidomini, Economic assessment of renewable energy systems integrating photovoltaic panels, seawater desalination and water storage, *Applied Energy* 253 (2019) 113575.
- [56] Y. Bai, Q. Bai, *Subsea engineering handbook*, Gulf Professional Publishing, 2018.
- [57] H. Fang, M. Duan, *Offshore operation facilities: equipment and Procedures*, Gulf professional publishing, 2014.
- [58] V. Narayanaswamy, Review of challenges in reliable electric power delivery to remote deep water enhanced oil recovery systems, *Applied Ocean Research* 43 (2013) 53–67.
- [59] N. Vedachalam, R. Ramesh, V. B. N. Jyothi, V. Doss Prakash, G. Ramadass, Autonomous underwater vehicles-challenging developments and technological maturity towards strategic swarm robotics systems, *Marine Georesources & Geotechnology* 37 (5) (2019) 525–538.
- [60] M. Ho, S. El-Borgi, D. Patil, G. Song, Inspection and monitoring systems subsea pipelines: A review paper, *Structural Health Monitoring* 19 (2) (2020) 606–645.
- [61] J.-E. Vinnem, et al., *Offshore risk assessment. vol. 1*, Springer Series in Reliability Engineering (2014).
- [62] M. Iannuzzi, A. Barnoush, R. Johnsen, Materials and corrosion trends in offshore and subsea oil and gas production, *npj Materials Degradation* 1 (1) (2017) 1–11.
- [63] T. Das, P. F. Tyvold, J. Jäschke, Modelling and optimization of compact subsea liquid-liquid separation system, in: *Computer Aided Chemical Engineering, Vol. 38, Elsevier, 2016*, pp. 1255–1260.
- [64] J. Plasencia, M. Andreotti, H. Wang, Z. Alam, Subsea seawater treatment and injection-performance tests of filtration membrane modules at simulated subsea conditions, in: *Offshore Technology Conference, OnePetro, 2018*.
- [65] A. Darmawan, J. P. Liyanage, Subsea asset maintenance on the ncs: On the trends, future innovation, and fitness of life-of-field,

- in: 9th WCEAM Research Papers, Springer, 2015, pp. 351–362.
- [66] E. Lachaud, Y. Monbeig, P. Nolleau, A. Hardy, M. Thompson, M. Lardeux, Opportunities and challenges of remote operating a rov embarked on a usv, in: Offshore Technology Conference, OnePetro, 2018.
- [67] F. Wen, J. Pray, K. McSweeney, H. Gu, Emerging inspection technologies—enabling remote surveys/inspections, in: Offshore Technology Conference, OnePetro, 2019.